Kinetic and Structural Characterization of Urease Active Site Variants[†,‡]

Matthew A. Pearson,[§,||] Il-Seon Park,[⊥,▽] Ruth A. Schaller,[⊥] Linda O. Michel,[⊥] P. Andrew Karplus,*[,#] and Robert P. Hausinger*[,⊥]

Departments of Microbiology and Biochemistry, Michigan State University, East Lansing, Michigan 48824, Section of Biochemistry, Molecular and Cell Biology, Cornell University, Ithaca, New York 14853, and Department of Biochemistry and Biophysics, Oregon State University, Corvallis Oregon 97331

Received March 17, 2000; Revised Manuscript Received May 12, 2000

ABSTRACT: *Klebsiella aerogenes* urease uses a dinuclear nickel active site to catalyze urea hydrolysis at $>10^{14}$-fold the spontaneous rate. To better define the enzyme mechanism, we examined the kinetics and structures for a suite of site-directed variants involving four residues at the active site: His320, His219, Asp221, and Arg336. Compared to wild-type urease, the H320A, H320N, and H320Q variants exhibit similar $\sim 10^{-5}$-fold deficiencies in rates, modest K_m changes, and disorders in the peptide flap covering their active sites. The pH profiles for these mutant enzymes are anomalous with optima near 6 and shoulders that extend to pH 9. H219A urease exhibits 10^3-fold increased K_m over that of native enzyme, whereas the increase is less marked ($\sim 10^2$-fold) in the H219N and H219Q variants that retain hydrogen bonding capability. Structures for these variants show clearly resolved active site water molecules covered by well-ordered peptide flaps. Whereas the D221N variant is only moderately affected compared to wild-type enzyme, D221A urease possesses low activity ($\sim 10^{-3}$ that of native enzyme), a small increase in K_m, and a pH 5 optimum. The crystal structure for D221A urease is reminiscent of the His320 variants. The R336Q enzyme has a $\sim 10^{-4}$-fold decreased catalytic rate with near-normal pH dependence and an unaffected K_m. Phenylglyoxal inactivates the R336Q variant at over half the rate observed for native enzyme, demonstrating that modification of non-active-site arginines can eliminate activity, perhaps by affecting the peptide flap. Our data favor a mechanism in which His219 helps to polarize the substrate carbonyl group, a metal-bound terminal hydroxide or bridging oxo-dianion attacks urea to form a tetrahedral intermediate, and protonation occurs via the general acid His320 with Asp221 and Arg336 orienting and influencing the acidity of this residue. Furthermore, we conclude that the simple bell-shaped pH dependence of k_{cat} and k_{cat}/K_m for the native enzyme masks a more complex underlying pH dependence involving at least four pK_as.

Urease (urea amidohydrolase, EC 3.5.1.5) catalyzes the deceptively simple hydrolysis of urea to form ammonia and carbamate. Many microorganisms use this reaction to provide a source of nitrogen for growth, and the enzyme plays an important role in plant nitrogen metabolism during the germination process (*1*, *2*). The presence of urease activity in soils is exploited in the widespread agricultural practice of urea-based fertilizer application for enhancing crop yields. Unfortunately, excessive levels of soil urease can degrade fertilizer urea too rapidly and result in phytopathic effects and loss of volatilized ammonia (*3*). Of medical and veterinary interest, urease is a virulence factor in certain human and animal pathogens; it participates in the development of kidney stones, pyelonephritis, peptic ulcers, and other disease states [reviewed in (*4*)]. In addition to the importance of urease to agriculture and medicine, the structure and catalytic mechanism of this enzyme are of interest because of its large enhancement (10^{14}-fold) of the rate of urea hydrolysis and the presence of active site nickel which is unique among hydrolytic enzymes.

Urease from jack bean seeds was the first enzyme crystallized (*5*); however, the protein structure was only recently elucidated using the enzyme from *Klebsiella aerogenes* (*6*). The bacterial urease is comprised of three subunits (11.1, 11.3, and 60.3 kDa) each present in three copies, resulting in a tightly packed trimer of trimers structure. The enzyme active site contains two nickel ions separated by ~3.6 Å and bridged by a lysine carbamate and a solvent molecule (*6*, *7*). A similar metallocenter is found in the homologous enzyme from *Bacillus pasteurii* (*8*); however, in that case, a protein flap that covers the active site in the

[†] This work was supported by the USDA (9803562 and earlier versions), by the NIH (DK45686), and by a Hoechst Marion Roussel fellowship and NIH training grant (GM08520) to M.A.P.

[‡] Coordinates for all structures have been deposited in the Brookhaven Protein Data Bank; urease variants and their access codes include the following: H320N, 1EJU; H320Q, 1EJV; H219N, 1EJS; H219Q, 1EJT; D221A, 1EJR.

* Correspondence should be addressed to R.P.H. at 160 Giltner Hall, Michigan State University, East Lansing, MI 48824 (phone: 517-353-9675; Fax: 517-353-8957; E-mail: Hausinge@pilot.msu.edu) or to P.A.K. at 2011 Agricultural & Life Sciences Building, Oregon State University, Corvallis, OR 97331 (phone: 541-737-3200; Fax: 541-737-0481; E-mail: karplusp@ucs.orst.edu).

[§] Cornell University.

[||] Current address: Laboratory of Molecular Biology, Building 5, NIDDK, NIH, Bethesda, MD 20892-0580.

[⊥] Michigan State University.

[▽] Current address: Division of Molecular Life Sciences and Center for Cell Signaling Research, Ewha University, Seoul, South Korea.

[#] Oregon State University.

10.1021/bi000613o CCC: $19.00
Published on Web 06/22/2000

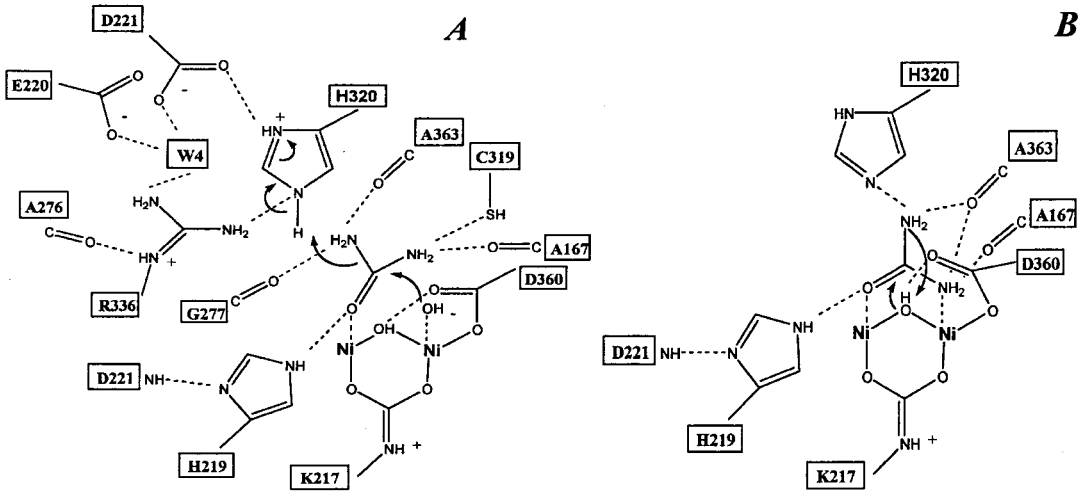

FIGURE 1: Mechanisms proposed for urease catalysis. (A) Working hypothesis proposed by Karplus et al. (*9*) based on studies with the *K. aerogenes* enzyme. (B) Proposal by Benini et al. (*8*) based on structural studies of *B. pasteurii* urease. The key residues in the mechanisms are shown using the *K. aerogenes* urease numbering scheme. The counterparts of Asp221, Gly277, and Arg336 in *B. pasteurii* urease also make similar interactions but were not discussed in the context of the second mechanism (*8*). In both panels, the bridging water molecule is WB, Ni-1 is depicted on the left and has W1 coordinated in the absence of urea, and Ni-2 is depicted on the right with W2 bound in substrate-free enzyme. In the absence of urea, a fourth active site solvent molecule is present, at the position taken by the amide interacting with His320, and referred to as W3. As shown, W4 is a bridge between Asp221 and Arg336. Asp360 is suggested to assist in proton transfer from WB to the departing urea amide group in the second proposal.

K. aerogenes enzyme is repositioned so as to expose the active site.

We have recently synthesized enzymological and structural information related to *K. aerogenes* urease to propose a detailed catalytic mechanism (*9*). As illustrated in Figure 1A, essential features of this mechanism are: (a) the urea carbonyl oxygen displaces water from and coordinates to Ni-1, with additional polarization provided by a hydrogen bond from His219, (b) a solvent molecule (with a pK_a of ~9) coordinated to Ni-2 attacks urea to form a tetrahedral intermediate, (c) His320 (located on the protein flap covering the active site and possessing a pK_a of ~6.5) acts to protonate the amido nitrogen, and finally (d) the protonated intermediate decomposes to form the products carbamate and ammonia. This model is proposed to operate by a "reverse protonation" mechanism in which the acid has a lower pK_a than the nucleophile, resulting in only a small proportion of enzyme being active at its pH maximum. Key evidence supporting this proposal are the active site geometry (*9*), the 10^5-fold reduction in turnover of the H320A variant of urease (*10*), the 10^3-fold increase in K_m of the H219A urease variant (*10*), the bell-shaped pH profiles of k_{cat} (and k_{cat}/K_m) with pK_a values of ~6.5 and ~9 for wild-type enzyme (*11*), and the assignment of the pK_a of 6.5 to His320 based on the pH dependence of inactivation by diethylpyrocarbonate (DEP)[1] combined with the observations that H320A urease is unaffected by DEP (*10*, *12*).

An alternative urease mechanism (Figure 1B) was proposed based on structural studies of the *B. pasteurii* enzyme (*8*). This model suggests that (a) urea binds in a chelating mode with its carbonyl oxygen coordinated to Ni-1 (stabilized by a residue equivalent to His219) and an amido group bound to Ni-2, (b) the Ni-bridging hydroxide (pK_a 9) attacks urea to form a tetrahedral intermediate with three positions bound to the dinuclear center, (c) the bridging hydroxide serves as the general acid (with Asp360 assisting in proton transfer) to donate a proton to the distal amino group, and (d) the residue equivalent to His320 acts to stabilize a positive charge in the transition state. Key evidence supporting this model is the structure of *B. pasteurii* enzyme with bound diamidophosphate (DAP), an inhibitor derived from the slow substrate phenylphosphorodiamidate (PPD) (*8*, *13*). The two oxygen atoms of DAP are bound at positions occupied by bridging and Ni-1 coordinated water molecules in the free enzyme, one DAP amido group is bound to Ni-2, and the other amido group is pointed away from the metallocenter. The proposed mechanism results from assuming that the bridging ligand oxygen is derived from the hydroxide that attacked PPD.

These two mechanisms agree on many points with the essential differences being the metal coordination geometry of the urea (O vs O and N ligation), the identity of the nucleophile (the Ni-2 bound vs bridging hydroxide), the identity of the acid (His320 vs the bridging hydroxide), and the protonation state of His320 (protonated vs deprotonated). Here, we continue to probe the urease mechanism by analyzing the enzyme kinetics and structures of additional variants involving His320 and His219, as well as Asp221 and Arg336 (two residues that may influence the properties of His320).

EXPERIMENTAL PROCEDURES

Site-Directed Mutagenesis and Recombinant DNA Methods. All mutagenesis efforts started with the 1.1-kb *Bam*HI−*Sal*I fragment of pKAU17 (*14*), a plasmid containing the *K. aerogenes ureDABCEFG* gene cluster. For generation of the H320N, H320Q, H219N, and H219Q variants of urease, the fragment was subcloned into M13mp18 and mutagenized (*15*), as previously reported for generation of the H320A and H219A variants (*10*). Uracil-containing single-stranded

[1] Abbreviations: DEP, diethylpyrocarbonate; DAP, diamidophosphate; PPD, phenylphosphorodiamidate; MES, 2-(*N*-morpholino)-ethanesulfonic acid; HEPES, *N*-(2-hydroxyethyl)piperazine-*N*′-2-ethanesulfonic acid; CAPS, 3-(cyclohexylamino)ethanesulfonic acid.

template DNA was prepared from *E. coli* CJ236 (*dut*1 *ung*1 *thi*-1 *rel*A1/pCJ105[*cam*^{r} F′]), and mutagenized phage were isolated in *E. coli* MV1193 (Δ[*lac*I-*pro*AB] *rpsL thi endA spcB*15 *hsdR*4 Δ[*srl*-*rec*A] 306::Tn10[*tet*^{r}] F′[*traD*36 *pro*AB$^+$ *lacI*^{q}*lacZ*ΔM15]). For generation of the D221A and R336Q variants, the *Bam*HI−*Sal*I fragment was subcloned into pBluescript KST and pUC19, respectively, and mutagenized by using the Morph kit (5-Prime→3-Prime). The following oligonucleotides were synthesized by using an Applied Biosystems Model 394 DNA synthesizer at the Michigan State University Macromolecular Structure Facility: GATGGTCTGCAACCATCTGG (H320N), GGTCTGCCAGCATCTGGAC (H320Q), CTGAAGATCAATGAGGACTGG (H219N), GAAGATCCAAGAGGACTGG (H219Q), GATCCATGAGGCATGGGGCGCCAC and GTGGCGCCCCATGCCTCATGGATC (D221A forward and reverse), GATCCATGAGGCATGGGGCGCCAC and GTGGCGCCCCATGCCTCATGGATC (D221N forward and reverse), and CTTTGCCGAGTCGCAGATTCGCCGCGAAAC (R336Q). Site-directed mutants were identified by restriction digest analyses or DNA sequencing and subcloned back into pKAU17 on *Mlu*I−*Bsm*I or *Mlu*I−*Bam*HI fragments. These regions were completely sequenced (*16*) to ensure that no other mutations had been introduced. The *Eco*RI−*Hin*dIII fragments of pKAU17 and several of its derivatives were cloned into similarly digested pKK223-3 (Pharmacia) to yield pKK17 and its variants. The urease genes are transcribed using the *tac* promoter in these constructs, resulting in routine high-level urease production.

Purification of Wild-Type and Variant Ureases. E. coli DH5α cells containing derivatives of pKAU17 (for isolation of the H320N, H320Q, H219N, and H219Q urease variants) were grown at 37 °C in LB medium containing 1 mM $NiCl_2$ and 100 μg/mL ampicillin. Similarly, *E. coli* HMS174(DE3) cells containing pKK17 and its derivatives (for purification of wild-type, D221A, D221N, and R336Q forms of urease) were grown at 37 °C in TB medium containing 1.5 mM $NiCl_2$, 1 mM IPTG, and 100 μg/mL ampicillin. After harvesting by centrifugation, the cells were disrupted, and the ureases were purified by described methods (*10, 17*). Much of the D221N protein was inactive and eluted from ion-exchange resins at lower salt concentrations than typically observed for wild-type enzyme. A second, minor form of this sample eluted at the normal position in the gradient and was found to be active. The inactive species was suspected to have folded aberrantly, and only the active species was further characterized. For proteins exhibiting negligible levels of activity, the urease-containing fractions were identified by sodium dodecyl sulfate−polyacrylamide gel electrophoresis (*18*).

Enzyme Assays. Urease activity for the wild-type enzyme was typically assayed in the presence of 25 or 50 mM HEPES, pH 7.75, buffer containing 0.5 mM EDTA and 50 mM urea. The levels of released ammonia were assessed in aliquots sampled at timed intervals by conversion to indophenol (*19*), and the rates were determined by linear regression analysis. Calculation of kinetic constants made use of the method of Wilkinson (*20*). Protein concentrations were measured by the method of Lowry et al. (*21*) or using the BioRad protein assay. Urease variants were assayed using modifications of this method, including the use of alternate buffers and pH to more closely match the pH optima of the variants and/or using 1 M urea for variants possessing low affinity for substrate. In all cases, the activities were examined over a range of pH values using the buffers indicated. When studying activities at low pH values, where the enzyme may be labile, time points were taken over short intervals, and the results are only reported if linearity of the reaction indicated that the values were not influenced by irreversible enzyme inactivation during the assay.

Fitting Procedure for pH Dependence Plots. In some cases, pH dependence plots were fit by assuming the presence of two pK_a values (pK_1 and pK_2) and a single V_{max} according to eq 1 that assumes the presence of saturating substrate concentrations:

$$v = \frac{V_{max}K_1[H]}{(K_1 + [H])(K_2 + [H])} \quad (1)$$

In other cases, however, the pH dependencies were more complex with one larger pH optimum along with a shoulder in the plots to higher or lower pH values. These data were fit to a 3-pK_a model that assumed activity depended on the protonation status of two groups with the maximum activity ranging from V_{max} to V_{max}' depending on the protonation status of a third group.[2] Data were fitted to this model using eq 2 that includes three macroscopic pK_a values (pK_1, pK_2, and pK_3).

$$v = \frac{V_{max}K_1K_2[H] + V_{max}'K_1[H]^2}{(K_1 + [H])(K_2 + [H])(K_3 + [H])} \quad (2)$$

In all cases, fitting was carried out using Kaleidagraph software (Synergy Corp.).

Chemical Modification Studies. Wild-type and R336Q ureases were subjected to chemical modification studies using phenylglyoxal. The enzymes were incubated at 37 °C in 80−100 mM HEPES buffer, pH 7.75, with 75 mM reagent, and timed aliquots were diluted into assay buffer to assess the activities remaining.

Crystallographic Methods. Crystals of H320N, H320Q, H219N, H219Q, and D221A urease were grown in space group $I2_13$ (a = 170.8 Å) as described for the nickel-bound wild-type enzyme (*22*). Diffraction data were mostly collected from single crystals at room temperature on an ADSC multiwire area detector and processed with Scalepack (*23*) (Table 1). For the D221A variant, two data sets were collected on an R-axis IV: one native and the other a 1 M formate soak. The formate soak showed no changes, so the data were merged into a single data set for the analysis (Table 1). The starting model for all refinements was a wild-type nickel-bound urease coordinate set refined at 1.9 Å resolution to an *R*-factor of 0.17 (M.A.P. and P.A.K., unpublished). This model is more accurate than the previously reported 2.2 Å structure [(*6, 7*) Protein Data Bank entry 1FWJ], but

[2] The complex pH profiles also were fit by assuming that they derived from the summation of two standard bell-shaped profiles. In the most general case, these fits provide two V_{max} and four pK_a values. The large number of variables associated with this approach led to large error ranges for some values. A simplified approach assumed that the two standard-shaped components comprising the overall pH profile shared one pK_a (either at one extreme of the profile or as the central value). This fitting approach led to more tightly defined pK_a values that matched those for the simple three-pK_a model.

Table 1: Crystallographic Data Collection and Refinement[a]

	H219N	H219Q	D221A[b]	H320N	H320Q
resolution (Å)	2.0	2.0	2.0	2.0	2.4
unique reflections	51963	52175	55503	49667	31070
completeness (%)	96 (64)	96 (67)	100 (100)	91 (60)	99 (98)
redundancy	2.9 (1.8)	2.9 (1.8)	10.8 (10.6)	2.3 (1.6)	2.7 (1.6)
R_{meas}	0.12 (0.55)	0.08 (0.38)	0.09 (0.58)	0.09 (0.46)	0.14 (0.42)
R_{mrgd-F}	0.16 (0.49)	0.12 (0.33)	0.07 (0.37)	0.14 (0.42)	0.17 (0.35)
R_{cryst}	0.185	0.173	0.161	0.187	0.181

[a] Values in parentheses correspond to data in the highest resolution bin as reported by RMEAS (*37*). [b] Two crystals were used for collecting this data set.

the architecture of the active site is nearly identical to that previously described. Difference electron density maps ($2F_o - F_c$ and $F_o - F_c$) were used to determine the position and extent of structural changes. In each case, refinement consisted of changing the mutated residue, manually adjusting the model in CHAIN (*24*), and removing the three Ni-coordinating waters before refining against all data between 10.0 Å and the nominal resolution limit. The conventional positional and restrained individual *B*-factor refinement protocols in X-PLOR 3.1 were used (*25*). After the first round of refinement, the Ni-bound waters were added back to the model as indicated in a difference map. Gln219 in the H219Q protein is present in two conformations whose occupancies were set to 0.67 and 0.33 (based on the visible density), and the atomic *B*-factors for each of these conformations were refined to values of 18−25 Å^2. The crystallographic models for H320N/Q, H219N/Q, and D221A urease variants were each refined to *R*-factors below 19% (Table 1). Following the lead of Benini et al. (*8*), key active site waters numbered 500, 501, 502, and 170 in our previous *K. aerogenes* structures have been renamed to WB (for bridging), W1 (terminally bound to Ni-1), W2 (terminally bound to Ni-2), and W3 (interacting with His320, WB, W1, and W2). A fifth active site water not discussed previously, water-158 in our earlier structures, has been renamed W4.

RESULTS

Improved Expression System. The native enzyme as well as the D221N/A and R336Q mutant proteins were isolated from recombinant *E. coli* HMS174(DE3) cells carrying derivatives of pKK17, a pKK223-3-based vector containing the *K. aerogenes* urease gene cluster. Use of the pKK17 plasmid constructs in this host overcame two significant shortfalls of the previously studied *E. coli* DH5α(pKAU17) system: (i) expression levels from the pKAU17 system varied widely compared to the consistently high-level expression noted using pKK17, and (ii) specific activities of purified urease isolated from *E. coli* DH5α(pKAU17) cells were typically 1400−1900 units·(mg of protein)$^{-1}$ [e.g., (*10*)] while that from *E. coli* HMS174(DE3)(pKK17) cells was a much improved 2150 ± 70 units·(mg of protein)$^{-1}$ (Table 2). The latter value is more similar to that of 2500 units·(mg of protein)$^{-1}$ for urease isolated from *K. aerogenes* (*17, 26*). Because the plasmids contain the same sequence of *K. aerogenes* DNA, we suspect the improvement in activity is due to subtle differences in the two *E. coli* hosts.

His320 Urease Variants. To better define the role of the putative catalytic acid His320, we present here more detailed kinetic analyses of H320A urease and the properties and structures of the H320N and H320Q variants. Asn and Gln were substituted for His320 because these residues can partially mimic the hydrogen-bonding properties of His, but not the acid/base properties.

Table 2: Kinetic Parameters of Wild-Type and Variant Recombinant Ureases[a]

urease variant	K_m (mM)	k_{cat}[b] (s^{-1})	assay conditions (buffer, pH)
wild-type	2.4 ± 0.1	2970 ± 100	HEPES, 7.75
H320A	10.9 ± 0.6	0.068 ± 0.003[c]	MES, 6.2
H320N	7.4 ± 0.5	0.060 ± 0.001[c]	MES, 6.2
H320Q	10.6 ± 1.0	0.033 ± 0.001[c]	MES, 6.2
H219A	2090 ± 630	194 ± 42[c]	HEPES, 7.75
H219N	175 ± 8	322 ± 6[d]	MES, 6.2
H219Q	227 ± 21	1860 ± 80[c]	MES, 6.2
D221N	3.6 ± 1.0	60 ± 5	HEPES, 7.75
D221A	24 ± 2.4	1.7 ± 0.03	MES, 5.1
R336Q	2.7 ± 0.3	0.62 ± 0.07	HEPES, 7.75

[a] Assays were carried out near the pH optima for each variant. [b] The k_{cat} is based on M_r = 83 000 for the urease catalytic unit. [c] Estimated from activity levels in cell extracts that contained urease as ∼10% of the total protein. [d] Estimated from activity in cell extracts that contained ∼5% urease.

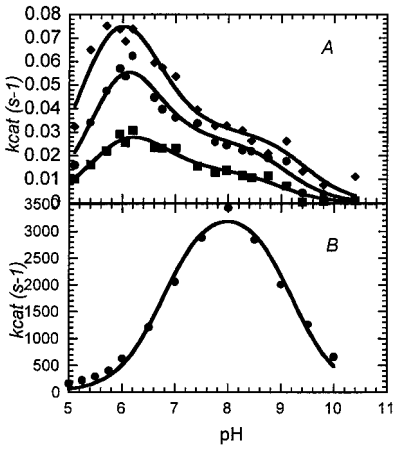

FIGURE 2: Effects of pH on His320 urease variant activities. (A) The H320A (●), H320N (◆), and H320Q (■) urease activities in cell extracts were measured using 25 mM MES (pH 5.1−6.2), HEPES (pH 6.0−9.1), and CAPS (pH 9.4−10.4) buffers containing 50 mM urea and 0.5 mM EDTA. Values of k_{cat} for the isolated enzymes were estimated by assuming the extracts contained urease as ∼10% of the total protein, and the data were fit to eq 2 to yield the parameters provided in Table 3. (B) The pH dependence of wild-type *K. aerogenes* urease provided for comparison.

The H320A, H320N, and H320Q variants all showed small changes in K_m and nearly 10^5-fold decreases in k_{cat} (Table 2). The pH profiles of activity for all variants were nearly identical and had pH optima shifted to near pH 6 (Figure 2A), compared to the wild-type urease optimum near pH 8 (Figure 2B). The shapes of the mutant urease plots were no

Table 3: Fitting of pH Profiles for Variant Ureases[a]

enzyme	lowest pK_a	middle pK_a	highest pK_a	V_{max} (units·mg^{-1})	V_{max}' (units·mg^{-1})
wild-type[b]	6.55	−	8.85	2500	−
H320A	⟨5.9⟩	⟨6.1⟩	9.2	0.018 ± 0.002	⟨0.13 ± 0.54⟩
H320N	5.3	6.5	9.5	0.022 ± 0.002	0.78 ± 0.012
H320Q	5.7	6.4	9.0	0.010 ± 0.001	0.04 ± 0.02
H219A[c]	6.7	−	9.4	62 ± 3	−
H219N[c]	4.6	7.7	9.5	114 ± 16	222 ± 6
H219Q[c]	5.1	7.6	9.4	480 ± 140	1040 ± 70
D221N	6.5	−	8.7	45.9 ± 3.1	−
D221A[d]	4.8	−	4.8	⟨1.84⟩	−
R336Q	≪5	6.8	9.1	0.045 ± 0.023	0.325 ± 0.015

[a] The H219A, D221N, and D221A data were fit according to eq 1, yielding a pair of pK_a values and a single V_{max}, whereas eq 2 was used for fitting the H320A, H320N, H320Q, H219N, H219Q, and R336Q data. The pK_a values typically have errors of approximately 0.3 pH unit. Values shown inside ⟨⟩ are associated with large errors. [b] Taken from (*11*). [c] Assayed in the presence of 1 M urea. [d] Assayed with 100 mM urea.

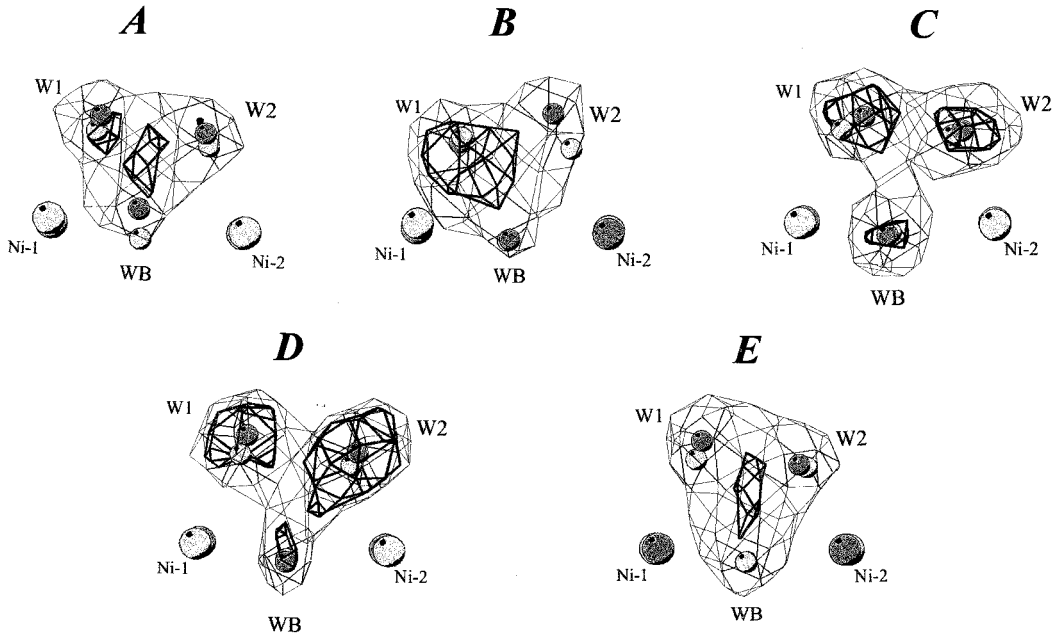

FIGURE 3: Nickel-bound water molecules. Overlays of the refined positions of the three nickel-bound water positions (W1, W2, and WB) are presented for variant ureases (dark gray) with wild-type urease (light gray). In addition, difference electron density (calculated with coefficients $F_o - F_c$ after removing the water molecules from the model) is shown at a low (thin lines) and a high (thick lines) contour level: (A) $4\rho_{rms}$ and $6\rho_{rms}$ for H320N, (B) $3\rho_{rms}$ and $4.5\rho_{rms}$ for H320Q, (C) $3\rho_{rms}$ and $5\rho_{rms}$ for H219N, (D) $3\rho_{rms}$ and $4\rho_{rms}$ for H219Q, and (E) $4\rho_{rms}$ and $8\rho_{rms}$ for D221A.

longer simple bell-shaped profiles, but showed a low pH maximum and a higher pH shoulder. The profiles were fit using eq 2 to provide three pK_a and two V_{max} values for each variant, as tabulated in Table 3.

The crystal structures of both the H320N and H320Q ureases revealed that no continuous density was visible for the active site flap containing residue 320, and residues 318−330 were not included in the models. We interpret this to mean that the flap becomes disordered and it is not possible to define discrete positions for Asn320 or Gln320 in the variants. In terms of the metal-bound water positions (Figure 3), the electron density for both mutants indicates that a constellation of three waters (WB, W1, and W2) still exists. However, because more density is present at a central position, it appears that in some molecules a single bridging water molecule may replace the three waters. For H320N, the modeled water molecules are shifted by 0.3−0.6 Å compared to the native enzyme. The W1 and W2 sites in H320Q are shifted by somewhat more, but the resolution of this structure is lower (2.4 Å vs 2.0 Å for the other variants), so these shifts partially reflect a larger positional error. Electron density maps and the refined coordinates indicated that no other active site residues have shifted significantly.

His219 Urease Variants. To test our hypothesis that the key role of His219 is to assist in substrate binding and not act as an acid or base, the H219A variant was subjected to further characterization, and the kinetics and structures of Asn and Gln variants at this position (H219N and H219Q) were characterized. Consistent with our previous results (*10*), the H219A variant had k_{cat}/K_m impaired by 10^4 compared to wild-type urease, with K_m increased by 10^3 and k_{cat} decreased by 15 (Table 2). In comparison to H219A urease, the H219N variant had about 20-fold higher catalytic efficiency largely due to a decrease in K_m, and H219Q urease had ca. 100-fold higher catalytic efficiency resulting from a 10-fold lower K_m and a 10-fold higher k_{cat} (Table 2). As shown in Figure 4, the three variant enzymes had distinct pH dependencies. The shape of the pH profile for H219A urease was similar to that found for wild-type enzyme, whereas the optima for H219N and H219Q were shifted to near pH 6 and each had

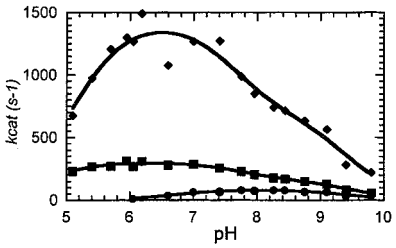

FIGURE 4: Effects of pH on His219 urease variant activities. The H219A (●), H219N (◆), and H219Q (■) urease activities in cell extracts were measured using 25 mM MES (pH 5.1−6.2), HEPES (pH 6.0−9.1), and CAPS (pH 9.4−10.4) buffers containing 1 M urea and 0.5 mM EDTA. Estimated k_{cat} values for purified enzymes were based on the presence of H219A and H219Q ureases comprising 10% of the protein in cell extracts, and H219N urease comprising 5% of the cell extract protein. The data were fit to eq 1 for H219A enzyme and to eq 2 for H219N and H219Q proteins yielding the parameters shown in Table 3.

a distinct shoulder much like what was observed for the His320 variants. These profiles were fit using eq 1 (for H219A urease) or eq 2 (for the H219N and H219Q variants) to obtain the pK_a and V_{max} values shown in Table 3.

The crystal structure of H219N urease revealed that Asn219 was well ordered with its Oδ1 atom structurally equivalent to His219 Nδ1 and receiving a hydrogen bond from the backbone nitrogen of Asp221 (Figure 5A). The H219Q structure showed Gln219 with a broad density that we have interpreted as two alternate conformations, one having Oϵ1 hydrogen bonded to the Asp221 backbone nitrogen and Nϵ2 hydrogen bonded to W1, and the other having Nϵ2 hydrogen bonded to the main chain carbonyl oxygen of Ala167 (Figure 5B). Aside from these unique features, the two structures showed three common changes. First, both variants possessed a slightly shifted and much more ordered flap, just as was seen for H219A urease (*27*), apourease (*27*), and C319A urease (*7*). The atomic *B*-factors of the flap residues were 13−40 Å^2 compared to >65 Å^2 in wild-type urease. A second common feature of the H219N and H219Q structures was that the electron density for waters WB, W1, and W2 was better resolved into three distinct peaks (Figure 3), indicating a less complex active site solvation structure than is present in wild-type urease. These water molecules were displaced about 0.5 Å from their wild-type positions, and the resulting water−water separations are 2.2−2.7 Å rather than the 1.9−2.1 Å values seen in wild-type urease. The shift in W1 was toward residue 219 to a position just ∼2.5 Å from the His219-Nϵ2 atom in wild-type urease. The hydrogen bond distances from Asn219-Nδ2 and Gln219-Nϵ2 were 3.6 and 2.6 Å, respectively. Coordinated with the changes involving W1 and W2 was a shift of 0.4 Å for W3, allowing it to make a 2.8 Å hydrogen bond to His320-Nϵ2. A third change common to the variants was a shift of the Asp221 carboxylate to fill space vacated by His219. Coordinated with this, W4 became better ordered and shifted in position.

Asp221 Variant Ureases. Whereas the D221N variant exhibited only modest activity changes in comparison to wild-type enzyme, D221A urease exhibited a 10-fold increase in K_m and a 10^3-fold decrease in rate (Table 2). The D221N enzyme exhibited a near-wild-type pH profile (Figure 6A), while maximal activity was observed at pH ∼4.8 using D221A urease (Figure 6B). Unlike the situation seen in the His320 variants that also exhibited low pH optima, the pH profile was extremely sharp, and no shoulder was observed toward higher pH for the D221A enzyme. The data were fit using eq 1 to obtain the pK_a and V_{max} values shown in Table 3.

The electron density for D221A urease clearly indicates the loss of the Asp221 side chain and disordering of the flap containing His320 (structure not shown). Although residual density and the *B*-factors of the surrounding residues suggest the flap is slightly more ordered that in the His320 variants, residues 318−330 have been removed from the model. Stronger density near the position occupied by the side chain of His320 may be due to a poorly ordered sulfate ion from the crystallization buffer. The only other active site change involved the binding of waters (WB, W1, and W2) to the nickel ions; maximum electron density was localized much more between the metals than found in the native enzyme (Figure 3). As for the His320 variant ureases (*27*), we interpret this to mean that a bridging hydroxide (or water) is present for many of the D221A urease molecules. Refinement with a single water site, however, could not account for the density, so we have still modeled it as a cluster of three water sites. Aside from the flap and the active site water molecules, no active site residue shifts significantly.

R336Q Urease. Arg336 makes an unusual interaction with His320 whereby an NH_2 proton points at the π-orbital of His320-Nϵ2. Arg336 was mutated to glutamine to remove its charge and interaction with His320, while allowing for the maintenance of a hydrogen-bonding interaction between Arg336-NE and Ala276-O. The R336Q variant possessed greatly reduced levels of activity compared to the control, with only moderate changes in K_m (Table 2). In contrast to the low pH optima observed for H219N, H219Q, D221A, and the three His320 variants, R336Q urease exhibited an optimum pH near 8.0 (Figure 7) as found for H219A, D221N, and wild-type enzymes. The pH profile, containing a shoulder toward lower pH values, was fit to eq 2 to provide the pK_a and V_{max} values shown in Table 3.

The presence of Arg336 in the active site recalled our earlier experiments showing urease activity was sensitive to reagents that modify arginine residues (*28*). In those studies, derivatization of urease by 2,4-pentanedione, 2,3-butanedione, or phenylglyoxal resulted in pseudo-first-order decreases in activity, with phenylglyoxal reacting at the greatest rate. That work also suggested a reactive arginine residue was present at the active site based on inhibitor competition studies. For example, β-mercaptoethanol, a competitive inhibitor of urease that binds to and bridges the dinuclear center (*29*), inhibited inactivation with the inactivation rate decreasing by 50% at ∼15 mM thiol (*28*). To test whether the sensitivity to arginine-specific reagents was due to the modification of Arg336, we carried out chemical modification studies on the R336Q variant. For this mutant enzyme, the pseudo-first-order rate of inactivation in the presence of 75 mM phenylglyoxal was 55% of that measured for native enzyme (0.0235 min^{-1} versus 0.0424 min^{-1}).

DISCUSSION

The goal of this work was to further examine the *K. aerogenes* urease mechanism by analyzing properties of

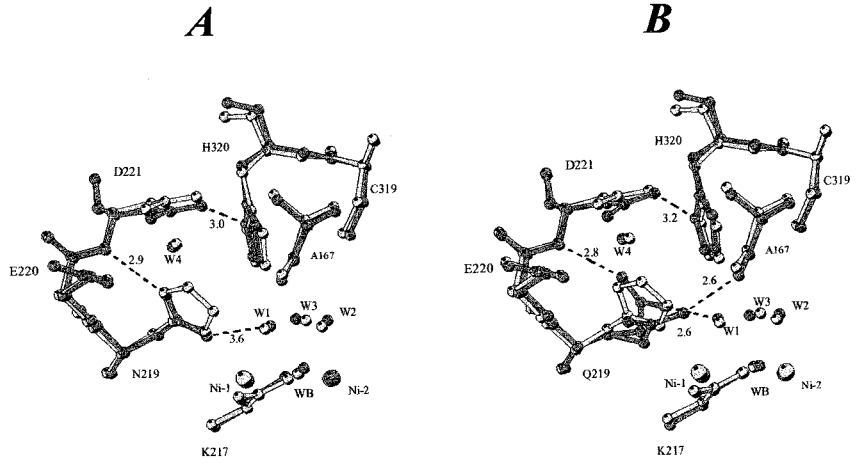

FIGURE 5: Active site structures of the H219N and H219Q variant ureases. Overlays of variants (dark gray) with wild-type urease (light gray) for H219N (A) and H219Q (B) ureases are presented with distances (in Å) for selected hydrogen bonds in the variants.

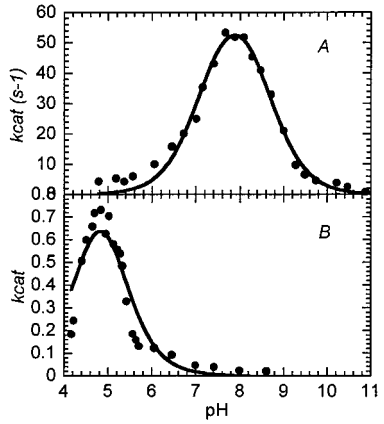

FIGURE 6: Effects of pH on Asp221 variant urease activities. D221N urease (A) was assayed in 50 mM buffers (acetate, MES, HEPES, EPPS, CHES, and CAPS over their respective ranges) containing 50 mM urea. Similarly, the D221A urease (B) was assayed in 50 mM acetate (pH 4.2−5.5), MES (pH 5.1−6.0), or HEPES (pH 6.4−8.6) buffers containing 250 mM urea. For both plots, the data were fit to eq 1.

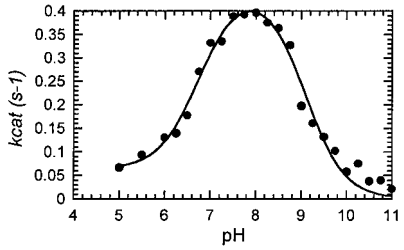

FIGURE 7: Effect of pH on R336Q urease activity. Purified R336Q urease was assayed in the presence of 25 mM MES (pH 5−6.5), HEPES (pH 6.75−8.75), CHES (pH 9−9.75), and CAPS (pH 10 and higher) buffers containing 50 mM urea and 0.5 mM EDTA.

selected site-directed enzyme variants involving His320, His219, Asp221, and Arg336. The latter two residues are located near to and interact with the key catalytic residue, His320. With one exception,[3] counterparts to His320, His219, Asp221, and Arg336 are found in all of the more than 30 urease sequences available in GenBank, attesting to their critical importance. Below, we discuss our results and how they impact our understanding the urease mechanism.

Role of His320. His320 was initially identified as a key residue based on the 10^5-fold reduction in rate (with little change in K_m) for the H320A variant compared to native urease (*10*). One proposed mechanism designates His320 as a proton donor, and the other assigns it to be a hydrogen bond acceptor that stabilizes a buildup of positive charge on the urea amide group (Figure 1). The properties of H320A do not distinguish between these roles because Ala is capable of neither of these functions. In contrast, Asn and Gln variants may distinguish between the models because these residues can participate in hydrogen bonding interactions that mimic the His nitrogens, but they cannot carry out acid/base catalysis. Indeed, since the amide side chain would be expected to be oriented with its NH_2 group toward Asp221, this would place the electronegative oxygen near the urea substrate where it could even provide improved stabilization of a positive charge buildup on the urea nitrogen. The properties of the H320N and H320Q variants were nearly indistinguishable from those of H320A urease, indicating that the presence of an amide side chain was not sufficient to restore urease activity. These results suggest strongly that the acid/base properties of His320 are required for its function. Nevertheless, a pure hydrogen bonding role of His320 is not precluded, because geometric limitations may hinder the amide-containing residues from mimicking the hydrogen bonding of His320 or may prevent the active site flap from closing properly in the presence of substrate. Indeed, the structures of all three mutant proteins show an open active site flap and some rearrangement of the Ni-bound waters.

Role of His219. His219 was originally identified as a key residue, as its mutation to Ala gave rise to a 10^3-fold increase in K_m with a moderate decrease in k_{cat} (*10*). Furthermore, urease structures from *K. aerogenes* (*6*, *7*) and *B. pasteurii* (*8*) indicate that His219 is appropriately positioned to donate a hydrogen bond to Ni-1-coordinated urea, thus facilitating substrate binding, but it is not properly located to act as an acid or base during catalysis. As with His320, we examined Asn and Gln variants at this position to assess the relative importance of hydrogen bonding and acid/base chemistry.

[3] The exception involves a partial urease sequence derived from a DNA amplification product of one isolate of *Helicobacter pylori* (strain KP72b; AB028036.1) in which Asp221 appears to be replaced by a serine; however, it is possible that a sequence error was introduced during PCR amplification.

Compared to H219A urease, H219N and H219Q variants had 20- and 90-fold improved values of k_{cat}/K_m. Although the major changes are in K_m, there are significant changes in k_{cat} as well. The structures of H219A, H219N, and H219Q all have a similarly rearranged flap and active site hydration, suggesting that activity differences are due to the specific hydrogen bonding of the side chain rather than the active site rearrangements. On the other hand, the pH profiles for the H219Q/N variants somewhat resemble those of the H320A/Q/N variants, hinting at a possible misorientation of His320 in these proteins. We conclude that His219 does not participate in acid/base catalysis, but does promote proper substrate binding by hydrogen bond donation and may influence the orientation of His320 to affect catalysis. The higher activity of H219Q correlates with the observation that its amide nitrogen is better able to mimic the placement of His219-Nϵ2 (Figure 5A vs 5B).

Role of Asp221. Our prior observation that Asp221 is hydrogen bonded to His320 (*6*, *7*), coupled with the importance of His320, led us to examine the role of this carboxylate residue in urease catalysis. Substitution of Asp221 by Asn led to only modest effects on activity, suggesting that the hydrogen bonding capability of the Asn is sufficient to maintain near-normal properties for His320. As demonstrated by the ~2000-fold reduction in activity of D221A urease compared to the wild-type enzyme, however, elimination of the side chain has dramatic effects. The structural analysis of D221A urease shows that the active site is rearranged similarly to the His320 mutants (flap open and more density associated with the bridging water), suggesting that Asp221 helps orient the imidazole of His320. Because the mutation to D221N did not alter the pH dependence despite the loss of a charge, we suggest this residue does not heavily influence the pK_a of His320.

Importance of Arginine Residues in Urease. As for Asp221, the close and unusual interaction of Arg336 with His320 (see Figure 1) led us to examine its role in urease catalysis. Substitution of Arg336 by glutamine reduces k_{cat} over 4000-fold with little effect on K_m. The observation that the R336Q urease pH optimum remained near that of wild-type enzyme indicates that the loss in activity is not simply due to a complete loss of function of His320, but instead is a more subtle effect that cannot be specified. Because phenylglyoxal inactivated the R336Q variant (where residue 336 is incapable of being modified) at over half of the rate measured for wild-type enzyme, Arg336 is not the only arginine whose modification affects activity. The phenylglyoxal-sensitive target(s) in the R336Q variant is(are) unclear, but additional arginines at positions 339 and 366 (interacting with Glu311) are exposed and located where their modification may affect the proper functioning of the active site flap.

Active Site Water Molecules. The structure of water molecules at the active site of urease differs for several of the variants compared to the native enzyme. In particular, the H320A (*27*), H320N, H320Q, and D221A structures all have a flap-open structure with what appears to be an enhanced presence of a single bridging water molecule replacing WB, W1, and W2 (Figure 3). The structures for these enzyme variants were determined at pH 7.5 where they are essentially inactive. As discussed for H320A urease (*27*), the lack of activity could be partly due to the reorganized hydration as well as the lack of or improper placement of His320. The activity generated at lower pH, especially in the case of D221A urease, may reflect protonation and possible rearrangement of the water structure at the active site.

The H219N and H219Q proteins exhibited an alternative water structure with the three metallocenter-bound water molecules being more clearly resolved and shifted apart from each other compared to the situation in native enzyme (Figure 3). These proteins also exhibit a slightly shifted and more well-ordered flap covering the active site, emphasizing a connection between metallocenter water structure and flap mobility. Interestingly, as with the apoenzyme (*27*) and the C319A variant (*7*), this reorganization is correlated with the removal of atoms from the active site: in the variants, atoms that belonged to the histidine or cysteine side chains are no longer present, and in the apoenzyme, the nickel ions are missing. As we have discussed (*9*), this connection suggests that the hydrated active site is a high-energy state with the bound water making suboptimal interactions (interactions worse than it would make in bulk solvent). In particular, the shift of W1 to a position that would have collided with the His219 side chain in the wild-type enzyme indicates that in native urease there exists a direct conflict between the location of the His219 and optimal hydration of the dinuclear nickel center. An intriguing possibility is that the more stable (relaxed) flap position observed in these mutant proteins may better approximate the structure adopted by wild-type enzyme in the presence of bound substrate. Indeed, in the His219 variant structures, His320 interacts better with Asp221 (3.0 Å vs 3.4 Å), and this interaction and the flap conformation are remarkably similar to the structure of *B. pasteurii* urease with the bound DAP inhibitor (*8*).

Analyses of the pH Profiles for Urease Variants. The pH profile for native *K. aerogenes* enzyme exhibits a typical bell-shape, providing pK_a values of 6.55 and 8.85 (*11*). It is commonly assumed that such a profile arises from the need for a deprotonated group of pK_a ~6.5 and a protonated group of pK_a ~9; however, the same profile can arise from the reverse situation, as we have proposed to be the case for urease (*9*). While one must exercise caution in interpreting pH dependence data (*30*), we suggest that comparison of the effects of pH on wild-type and mutant ureases is mechanistically relevant and worthy of detailed discussion.

Our mutant urease studies show that the 2-pK_a model is an oversimplification. For many of the mutant enzymes, removal of an ionizable residue at the active site led to pH profiles requiring a minimum of three pK_a values for fitting. Thus, at least four ionizable groups appear to work in concert to generate the pH profile of native urease. Given the presence of several ionizable residues at the active site (His320, Asp221, Arg336, Cys319, and others) as well as three ionizable metal-bound water molecules (with the bridging WB capable of three ionization states: fully protonated, hydroxide, and the oxo-dianion), a complex pH effect is plausible. Also, other wild-type ureases provide examples of pH profiles that do not fit the prototypical 2-pK_a model. For jack bean urease, the complicated pH dependence of k_{cat} was modeled with two maximum rates and three pK_as (3, 6.25, and 9.0) (*31*). Profiles exhibiting distinct optima near pH 8 accompanied by shoulders to lower pH values also have been reported for ureases from *Helicobacter pylori*

(*32*) and *Schizosaccharomyces pombe* (*33*). Furthermore, the pH profile of soybean leaf urease possesses distinct optima at pH 5.25 and 8.75 (*34*).

We propose that the apparently simple pH dependence of *K. aerogenes* urease arises from the critical roles played by two ionizable groups, His320 and the metal-bound nucleophilic water molecule, with numerous other ionizable groups modulating these pK_as. The effects of these other groups are brought out in the mutant enzymes where a critical group is removed or perturbed in its properties. The pH dependence of the His320 variants is most open to interpretation because direct substitution of a putative catalytic group can lead to profound changes in the enzyme properties. The trace levels of activity remaining in the H320A, H320Q, and H320N enzymes are consistent with a requirement for groups of pK_a <6 and ~9, with another group of pK_a 6−6.5 modulating the V_{max}. We refrain from attempting to assign these pK_a values because both the flap covering the active site and the metal-bound water structure are perturbed at neutral pH compared to the native enzyme. Mutants affected at His219 retain much higher levels of activity, consistent with a less dramatic perturbation to the catalytic groups. Whereas the pH profile of H219A urease resembles that of wild-type enzyme, the H219N and H219Q pH profiles are similar to those of the His320 variants. The resulting low pH maximum and shoulder extending to higher pH may correlate with the shift of Asp221 closer to the position normally occupied by His219 and away from His320 in the H219N and H219Q ureases. Diminishment of the Asp221−His320 interaction would be expected to decrease the pK_a of the histidine residue, in accordance with the shift of the lowest pK_a from pH 6.5 in native enzyme to pH 4.6−5.0 in these mutant proteins. A similar shift of the lower pK_a (to pH 4.8) was noted in D221A urease where the Asp221−His320 interaction is precluded. In this case, however, the pH profile did not include a shoulder extending to pH ~9. We suspect that this high pH change corresponds to the distinct water structure of the active site in this variant. Finally, for R336Q urease, elimination of the guanidinium group that normally interacts with His320 is expected to lead to an increase in pK_a of the imidazole. Compatible with this interpretation, the lower pK_a of the R336Q pH profile exhibits a modest increase over that reported for the native enzyme.

Mechanistic Implications. The active site geometries are very similar in the DAP complex of *B. pasteurii* urease and various forms of *K. aerogenes* urease (especially the H219N and H219Q variants); however, this consensus does not resolve the discrepancies between the currently proposed mechanisms regarding the docking mode of urea, the identity of the nucleophile, and the identity of the catalytic acid. These three issues are discussed within the context of our currently preferred urease mechanism, illustrated in Figure 8, that merges selected aspects of the two prior mechanisms.

Given the plausible assumption that DAP binds as a transition state analogue (*8*), then urea would bind as shown in Figure 1B, and WB must serve as the nucleophile. While this is the most direct interpretation of the data, two arguments lead us to consider the possibility that DAP binding does not reliably represent the transition state, and that other docking modes [including that shown in Figure 1A and a carbonyl oxygen-bridging mode as reported for a dinuclear model compound (*35*)] should not be ruled out.

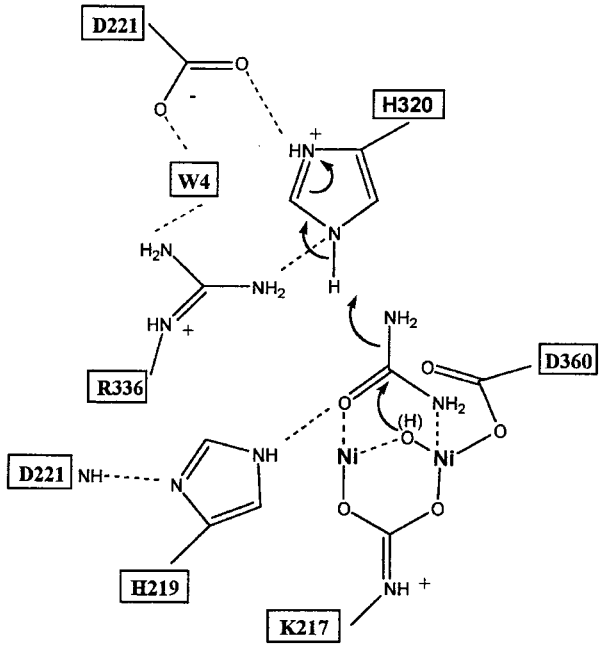

FIGURE 8: Revised reverse-protonation mechanism for urease. The urea carbonyl oxygen is proposed to bind to Ni-1 with additional polarization provided by a hydrogen bond from His219. Following nucleophilic attack by metal-bound solvent (pK_a ~9) and proton donation by His320 (pK_a ~6.5), the tetrahedral product decomposes to the products ammonia and carbamate. It is unclear whether a urea amido group also binds to Ni-2, as shown, so that resonance stabilization can be overcome by strong interactions with the π-electrons of each urea nitrogen: one lone pair ligated to Ni-2 and the other accepting a hydrogen bond from His320. Also unknown is whether urea binding weakens the interaction between Ni-1 and WB, forming a terminally coordinated water site, or if WB remains bridged to the two metals. The apparently simple bell-shaped pH profile for native urease belies an underlying complexity in the pH dependence, with Asp221, Arg336, Cys319 (*38*), and perhaps other ionizable residues affecting catalysis.

The first argument is that the bound DAP results from the hydrolysis of PPD, which is a tetrahedral (rather than trigonal) substrate and has a bulky phenyl group that cannot fit into a closed active site. Thus, PPD hydrolysis must occur from a geometry that does not mimic urea: the flap must be open and, since the leaving group (phenol) is not an NH_2-group as it is in urea, either the leaving group or the NH_2 must be bound in a nonrepresentative position. A second point is that DAP itself is only a relatively weak inhibitor, and this would not be expected for a true transition state analogue. Our results support urea binding to Ni-1 with polarization provided by His219, but they do not address whether W2 remains bound or is replaced by one urea amide as proposed by Benini et al. (*8*). In Figure 8, we adopt the latter scenario because it provides a chemically attractive rationale for removing much of the 30−40 kcal/mol of resonance stabilization energy associated with urea. In this scenario, the π-electrons of both urea nitrogens are engaged in strong electron-withdrawing interactions, as is the urea oxygen, leaving the central carbon rather electron-poor and primed for nucleophilic attack.

Our studies of variant ureases do not allow us to identify which metal-bound solvent is the nucleophile; however, reactivity studies involving inorganic complexes (*35*), the structure of DAP-inhibited *B. pasteurii* enzyme (*8*), and the results of recent fluoride inhibition studies of *K. aerogenes*

urease (*36*) lead us to favor WB as the nucleophile. If urea binding leads to a weakening of the WB·Ni-1 interaction, thus converting WB to a terminal ligand of Ni-2, the nucleophilic hydroxide would be expected to possess a pK_a of approximately 9. Similarly, a pK_a near 9 is expected for formation of the nucleophilic oxo-dianion species of WB on the basis of results for a dinuclear nickel complex in which a bridging water was successively deprotonated at pH 4.38 and 8.51 (*35*). Thus, we assign WB as the nucleophile (pK_a ~9) in urease catalysis.

With regard to the catalytic acid, we find that the kinetic and structural studies described above are most compatible with His320 serving as a general acid with a pK_a of ~6.5, as shown in Figure 1A. A serious problem with the Benini proposal, where WB acts as the proton donor via Asp360, is that the Asp360 carboxylate is bound to the metal so that only the carbonyl group is available to assist in proton transfer. We view this possibility as being highly unlikely. In summary, the pH dependence of wild-type urease is consistent with a reversed protonation mechanism in which terminally bound hydroxide (formed upon urea binding) or the bridging oxo-dianion of WB (pK_a ~9) acts with the general acid His320 (pK_a ~6.5) to achieve catalysis (Figure 8).

ACKNOWLEDGMENT

We thank Matt Todd for carrying out the initial arginine modification studies with wild-type enzyme, and Stefano Ciurli for providing the coordinates of the *B. pasteurii* urease structures prior to their release from the Protein Data Bank.

REFERENCES

1. Mobley, H. L. T., and Hausinger, R. P. (1989) *Microbiol. Rev. 53*, 85−108.
2. Zonia, L. E., Stebbins, N. E., and Polacco, J. C. (1995) *Plant Physiol. 107*, 1097−1103.
3. Mulvaney, R. L., and Bremner, J. M. (1981) in *Soil Biochemistry* (Paul, E. A., and Ladd, J. N., Eds.) pp 153−196, Marcel Dekker, Inc., New York.
4. Mobley, H. L. T., Island, M. D., and Hausinger, R. P. (1995) *Microbiol. Rev. 59*, 451−480.
5. Sumner, J. B. (1926) *J. Biol. Chem. 69*, 435−441.
6. Jabri, E., Carr, M. B., Hausinger, R. P., and Karplus, P. A. (1995) *Science 268*, 998−1004.
7. Pearson, M. A., Michel, L. O., Hausinger, R. P., and Karplus, P. A. (1997) *Biochemistry 36*, 8164−8172.
8. Benini, S., Rypniewski, W. R., Wilson, K. S., Miletti, S., Ciurli, S., and Mangani, S. (1999) *Structure 7*, 205−216.
9. Karplus, P. A., Pearson, M. A., and Hausinger, R. P. (1997) *Acc. Chem. Res. 30*, 330−337.
10. Park, I.-S., and Hausinger, R. P. (1993) *Protein Sci. 2*, 1034−1041.
11. Todd, M. J., and Hausinger, R. P. (1987) *J. Biol. Chem. 262*, 5963−5967.
12. Park, I.-S., and Hausinger, R. P. (1993) *J. Protein Chem. 12*, 51−56.
13. Andrews, R. K., Dexter, A., Blakeley, R. L., and Zerner, B. (1986) *J. Am. Chem. Soc. 108*, 7124−7125.
14. Mulrooney, S. B., Pankratz, H. S., and Hausinger, R. P. (1989) *J. Gen. Microbiol. 135*, 1769−1776.
15. Kunkel, T. A., Roberts, J. D., and Zakour, R. A. (1987) *Methods Enzymol. 154*, 367−382.
16. Sanger, R., Mickle, S., and Coulson, A. R. (1977) *Proc. Natl. Acad. Sci. U.S.A. 80*, 3963−3965.
17. Todd, M. J., and Hausinger, R. P. (1989) *J. Biol. Chem. 264*, 15835−15842.
18. Laemmli, U. K. (1970) *Nature (London) 227*, 680−685.
19. Weatherburn, M. W. (1967) *Anal. Chem. 39*, 971−974.
20. Wilkinson, G. N. (1961) *Biochem. J. 80*, 324−332.
21. Lowry, O. H., Rosebrough, N. J., Farr, A. J., and Randall, R. J. (1951) *J. Biol. Chem. 193*, 265−275.
22. Jabri, E., Lee, M. H., Hausinger, R. P., and Karplus, P. A. (1992) *J. Mol. Biol. 227*, 934−937.
23. Otwinowski, Z. (1993) in *Data Collection and Processing* (Sawyer, L., Isaacs, N., and Bailey, S. S., Eds.) SERC Daresbury Laboratory, Warrington, U.K.
24. Sack, J. S. (1988) *J. Mol. Graphics 6*, 224−225.
25. Brünger, A. T. (1993) *X-PLOR, version 3.1*, Yale University Press, New Haven, CT.
26. Todd, M. J., and Hausinger, R. P. (1991) *J. Biol. Chem. 266*, 24327−24331.
27. Jabri, E., and Karplus, P. A. (1996) *Biochemistry 35*, 10616−10626.
28. Todd, M. J. (1991) Ph.D. Thesis, Michigan State University, East Lansing, MI.
29. Benini, S., Rypniewski, W. R., Wilson, K. S., Ciurli, S., and Mangani, S. (1998) *J. Biol. Inorg. Chem. 3*, 268−273.
30. Knowles, J. R. (1976) *Crit. Rev. Biochem. 4*, 165−173.
31. Dixon, N. E., Riddles, P. W., Gazzola, C., Blakeley, R. L., and Zerner, B. (1980) *Can. J. Biochem. 58*, 1335−1344.
32. Evans, D. J., Jr., Evans, D. G., Kirkpatrick, S. S., and Graham, D. Y. (1991) *Microb. Pathog. 10*, 15−26.
33. Lubbers, M. W., Rodriquez, S. B., Honey, N. K., and Thornton, R. J. (1996) *Can. J. Microbiol. 42*, 132−140.
34. Kerr, P. S., Blevins, D. G., Rapp, B. J., and Randall, D. D. (1983) *Physiol. Plant. 57*, 339−345.
35. Barrios, A. M., and Lippard, S. J. (1999) *J. Am. Chem. Soc. 121*, 11751−11757.
36. Todd, M. J., and Hausinger, R. P. (2000) *Biochemistry 39*, 5389−5396.
37. Diederichs, K., and Karplus, P. A. (1997) *Nat. Struct. Biol. 4*, 269−275.
38. Martin, P. R., and Hausinger, R. P. (1992) *J. Biol. Chem. 267*, 20024−20027.

BI000613O